We are IntechOpen, the world's leading publisher of Open Access books Built by scientists, for scientists

4,800
Open access books available

122,000
International authors and editors

135M
Downloads

Our authors are among the

154
Countries delivered to

TOP 1%
most cited scientists

12.2%
Contributors from top 500 universities

CLARIVATE ANALYTICS BOOK CITATION INDEX INDEXED

WEB OF SCIENCE™

Selection of our books indexed in the Book Citation Index in Web of Science™ Core Collection (BKCI)

Interested in publishing with us?
Contact book.department@intechopen.com

Numbers displayed above are based on latest data collected.
For more information visit www.intechopen.com

23

Novel Pressure - Induced Structural Transformations of Inorganic Nanowires

Yang Song and Zhaohui Dong
Department of Chemistry, University of Western Ontario
Canada

1. Introduction

Nanostructured materials in different morphologies such as dots, wires and belts are of fundamental importance because of their wide range of tunable electrical, optical and mechanical properties that the bulk materials do not possess. These properties that critically depend on the nano-structures predominantly determined by the synthetic approaches, however, can be substantially modified by compression (Chen et al., 2002; Chen & Herhold, 1997; Guo et al., 2008; He et al., 2005; Jacobs et al., 2001; Jiang & Gerward, 2000; Jiang et al., 1999; Jiang et al., 2001; Jiang et al., 1998; Park et al., 2008; Swamy et al., 2006; Tolbert & Alivisatos, 1994; Tolbert & Alivisatos, 1995; Wang et al., 2005; Wang et al., 2001). Investigations of the structures and phase transformations of nanomaterials under high pressures have received increasing attention simply because high pressure has proven to be a powerful driving force to produce new structures and, therefore, new nanomaterial properties (San-Miguel, 2006). The most interesting aspect of high-pressure studies on nanomaterials is the observation that compressed nanomaterials exhibit significantly different behaviours than their corresponding bulk counterparts, such as the size-dependent phase transformations observed for nano-scale CdSe (Tolbert & Alivisatos, 1994; Tolbert & Alivisatos, 1995), SnO_2 (He et al., 2005; Jiang et al., 2001) and TiO_2 (Swamy et al., 2006). In addition, morphology can play an important tuning role in the pressure-induced transformations of nanostructured materials. For instance, ZnS nanobelts have been found to exhibit a much wider stability region up to 6.8 GPa for the wurtzite phase, in strong contrast to bulk ZnS, which is much more stable in the sphalerite phase (Wang et al., 2005).

In this chapter, we focus our interests on one-dimensional inorganic nanostructured materials, such as nanowires, due to their wide range of applications. Table 1 summarizes all high-pressure studies on one dimensional inorganic nanomaterials so far. In particular, we will discuss the novel and unusual pressure behaviors of two inorganic nanowires with great technological importance: tin dioxide (SnO_2) and gallium nitride (GaN). Our findings in these studies demonstrate the potential of using the combination of pressure and morphology as a powerful approach to tune the structures and properties of one-dimensional nanomaterials required for specific applications.

Material	Morphology	Dimension *	Pressure (GPa)	Characterization Method	Reference
ZnS	Nanobelt	*t*: ~10 nm *w*: ~1 μm *l*: 100 μm	0-11.4	X-ray diffraction	(Wang et al., 2005)
	Nanorod	*w*: ~10 nm	0-19.4	Raman, Photoluminescence	(Li et al., 2007)
		w: ~10 nm	0-37.2	X-ray diffraction	(Li et al., 2011)
BN	Nanotube	*d*: 20-50 nm	0-16	Raman	(Saha et al., 2007; Saha et al., 2006)
		d: ~ 50 nm	0-19.1	X-ray diffraction	(Muthu et al., 2008)
		d: ~ 100 nm	0-34.6	FTIR	(Dong & Song, 2010)
ZnO	Nanowire	*w*: 60-100 nm *l*: tens of μm	0-21.5	Raman, X-ray diffraction	(Yan et al., 2009)
	Nanotube	*d*:10-70 nm	0-21.5	X-ray diffraction	(Hou et al., 2009)
SnO_2	Nanowire	*w*: 50-60 nm *l*: several μm	0-37.9	Raman, X-ray diffraction	(Dong & Song, 2009)
	Nanobelt	*t*: tens of nm *w*: ~1μm *l*: several μm	0-36.2	Raman, X-ray diffraction	(Dong & Song, 2009)
TiO_2	Nanoribbon	*t*: ~20 nm *w*: 50-200 nm *l*: tens of μm	0-30.9	Raman, X-ray diffraction	(Li et al., 2010)
GaN	Nanowire	*w*: tens of μm *l*: < 100 nm	0-65	X-ray diffraction	(Dong & Song, 2010)

Table 1. Summary of high-pressure studies on one-dimensional inorganic nanomaterials.
* *d*: diameter; *w*: width; *l*: length; *t*: thickness

2. Experimental details

2.1 Materials

SnO_2 nanobelts and nanowires were synthesized using chemical vapor deposition on silicon substrate, starting with SnO powders (99%, Alfa Aesar). The experimental details have been described elsewhere (Wang et al., 2007; Zhou et al., 2006). The morphologies and chemical composition of SnO_2 nanobelts and nanowires were examined by scanning electron microscopy (SEM) (Instrument model: Leo/Zesis 1540XB FIB/SEM) and energy dispersive X-ray spectroscopy. Fig. 1a and 1c show the dimensions and morphologies of the as-made SnO_2 nanobelts and nanowires. The nanobelts are several tens of nanometers thick, several micrometers long and a few hundred nanometers up to 1 μm wide. The nanowires were 50-60 nm in diameter and several microns long.

The GaN nanowires were synthesized by passing ammonia through a mixture of Ga and Ga_2O_3 at high temperature in the presence of Au nanoparticles as the catalysts. The experimental details were reported previously (Zhou et al., 2005). The nanowires were thoroughly characterized by SEM. The SEM images (Fig. 2) reveal that the GaN nanowires have wire-like structure with zigzag periodic units. Most of the wires have a length of tens to hundreds of microns and their thickness is several tens of nanometers.

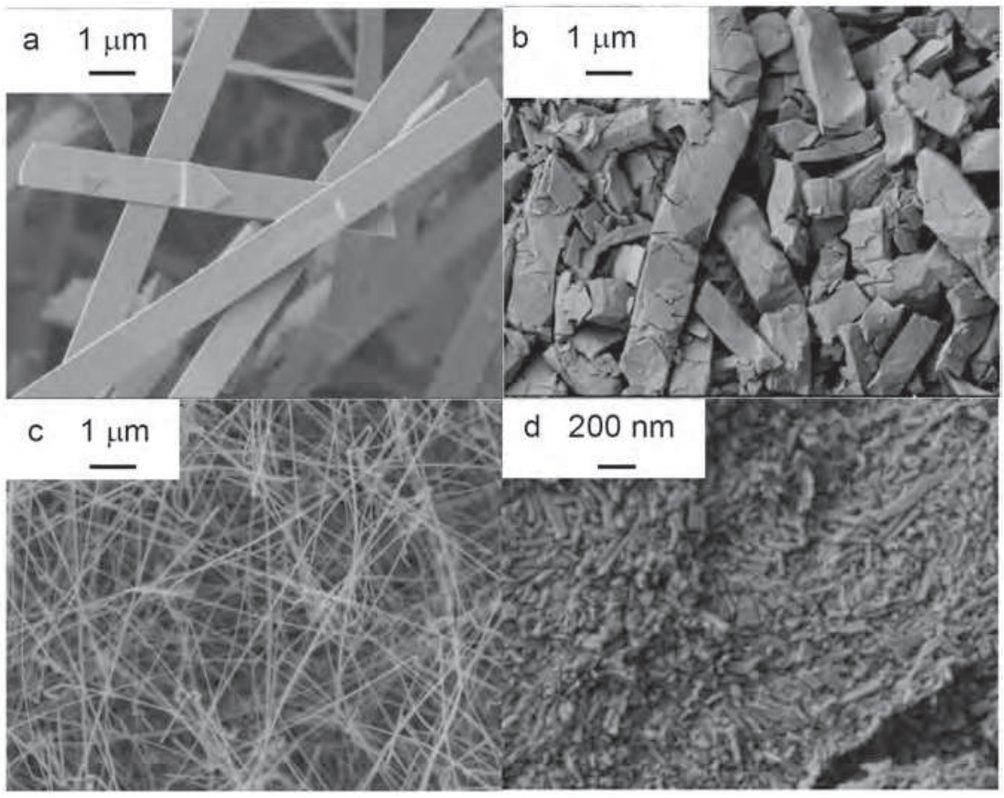

Fig. 1. SEM images of SnO_2 nanobelts before compression (a) and after decompression (b) as well as SnO_2 nanowires before compression (c) and after decompression (d) with scales shown in each panel. (From Dong & Song, 2009)

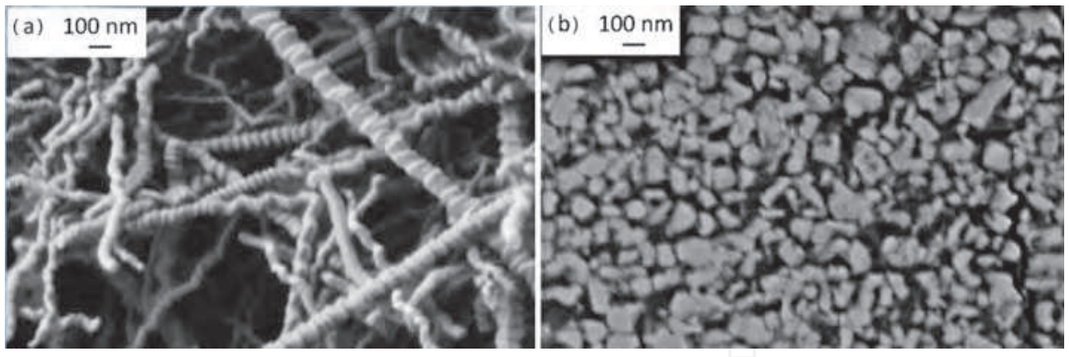

Fig. 2. SEM images of GaN nanowires before compression (a) and after decompression (b) with scales labeled in each panel. (From Dong & Song, 2010).

2.2 High pressure techniques

Diamond anvil cell (DAC) is a fundamental apparatus to achieve static high pressures. Recent rapid advances in the DAC technology have allowed the generation of extreme conditions in a broad P-T range with great controllability and accuracy (Hemley & Mao, 2002). The transparency of diamonds over a wide wavelength range allows the use of various optical techniques to examine the high-pressure behaviors of materials in situ. Over

the past a few decades, in particular, new emerging analytical probes including optical spectroscopy, synchrotron and neutron sources have enabled structural characterization of materials with unprecedented spatial, temporal and spectral resolutions (Hemley & Mao, 2002).

Fig. 3 shows a typical DAC apparatus where two brilliant cut diamonds are used as anvils to exert static pressure up to several million atmospheres (or several hundred GPa) with only moderate force. Such extreme pressures can be accurately determined by monitoring ruby fluorescence lines using the following relationship (Mao et al., 1978):

$$P = \frac{1904}{B}\left[\left(1+\frac{\Delta\lambda}{694.24}\right)^{B}-1\right] \quad (1)$$

where P is the pressure in GPa, $\Delta\lambda$ is the ruby R_1 line shift in nm, and parameter B is 7.665 for quasi-hydrostatic conditions and is 5 for non-hydrostatic conditions.

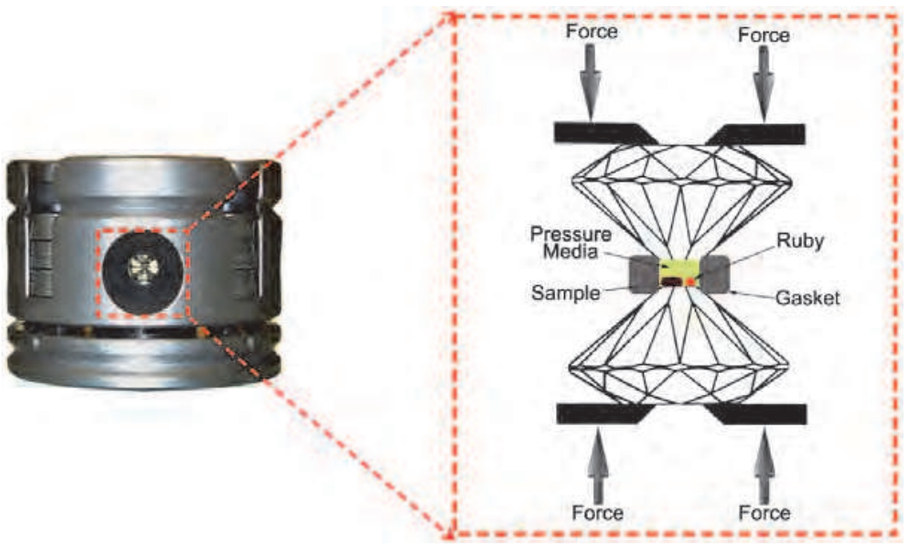

Fig. 3. Photo and schematics of a symmetric diamond anvil cell.

In the experiment for SnO_2 nanomaterials, a symmetric DAC with a pair of type I diamonds and a 400-micron culet was used. A hole with a diameter of 150 microns was drilled on a stainless steel gasket and used as the sample chamber. A few ruby chips were loaded with the sample as the pressure calibrant. The samples were loaded without pressure transmitting medium (PTM) for Raman measurements, whereas silicon oil was used as the PTM for X-ray diffraction measurements. GaN nanowires were compressed up to 65 GPa using a symmetric diamond anvil cell (DAC) which consists of a pair of type I diamonds with 200 μm culets and cubic boron nitride seats. The sample and a small ruby ball were enclosed in an 80-μm-diameter hole in a tungsten gasket. Silicone oil was used as the PTM.

2.3 In situ Raman spectroscopy

Vibrational spectroscopies compatible with DAC apparatus, including Raman and Fourier Transform Infrared (FTIR) microspectroscopy have been widely used to characterize high-

pressure structures of materials in situ. In particular, Raman spectroscopy is a sensitive structural characterization probe providing rich information about molecular geometries, bonding properties, phase identities and transformations, lattice dynamics, and crystallinity of materials, etc. Raman measurements were performed on SnO_2 nanobelts using a customized Raman micro-spectroscopy system. A 488 nm line from an Innova Ar^+ laser (Coherent Inc.) was used as the excitation source and was focused to less than 5 μm on the sample by an Olympus microscope. The Rayleigh line was removed using a pair of notch filters. The scattered light was dispersed using an imaging spectrograph equipped with a 1800 lines/mm grating, achieving a resolution of 0.1 cm^{-1}. The scattered light was then recorded using an ultrasensitive liquid-nitrogen-cooled, back-illuminated charge-coupled device (CCD) detector from Acton. The system was calibrated using neon lines with an uncertainty of ± 1 cm^{-1}.

2.4 Synchrotron X-ray micro-diffraction

Synchrotron light source in the high-energy hard X-ray region is an indispensable probe for DAC based materials characterizations. Such hard X-ray available in almost all synchrotron facilities worldwide enables in situ diffraction measurements on micron-sized materials under extreme P-T conditions with unparalleled accuracy for the elucidation of crystalline structures. For SnO_2 nanomaterials, the angle dispersive X-ray diffraction measurements were carried out at the X17C beamline at the National Synchrotron Light Source (NSLS) at Brookhaven National Laboratory (BNL). A high-energy, fixed-exit monochromator with Sagittelly-bent double Si crystal Laue mode was used to optimize the high-energy synchrotron X-ray from 20 keV to 40 keV, with an incident X-ray wavelength of 0.4066 Å. A pair of Kirkpatrick-Baez (KB) mirrors consisting of Si crystals coated with Pt and a focal length of 100 mm was used to focus the white X-ray beam at a glancing angle of approximately 1 mrad. This focused a 180 μm×180 μm incident beam to a 25 μm (horizontal) × 25 μm (vertical) beam on the sample. A MAR CCD X-ray detector was used to collect the 2D Debye-Scherrer patterns. The gonioemeter geometry and other diffraction parameters were calibrated using CeO_2 standard diffraction. Each diffraction pattern was obtained during an average exposure time of 5 to 10 minutes. The two-dimensional Debye-Scherrer patterns were converted to one-dimensional diffraction patterns using Fit2D software and Rietveld refinements were performed using GSAS package.

The angle-dispersive X-ray diffraction measurements on GaN nanowires were performed at the undulator sector 16-ID-B, High-Pressure Collaborative Access Team (HPCAT), Advanced Photon Source (APS) of Argonne National Laboratory (ANL) using an incident wavelength of 0.3680 Å and beam size of 15 μm×10 μm. The procedures of data analysis for GaN nanowires are similar to those for SnO_2 nanomaterials.

3. SnO_2 nanobelts and nanowires under high pressures

3.1 Properties, structures, and applications of SnO_2

As an *n*-type semiconductor with a large band gap (E_g = 3.6 eV at 300 K), SnO_2 has been studied extensively for applications in transparent conducting electrodes, lithium ion batteries and gas sensors (Watson et al., 1993). Specifically, because SnO_2 exhibits high sensitivity for detecting CO and NO_x gases, vigorous studies on SnO_2-based gas sensors

have been undertaken (Watson et al., 1993). In these studies, SnO_2 in orthorhombic structures was found to exhibit better sensitivity for specific gases than the tetragonal rutile-type structure (Arbiol et al., 2008; Sangaletti et al., 1997). However, natural SnO_2, known as cassiterite, always exists as the rutile-type structure and it is generally difficult to obtain the orthorhombic phase directly from minerals (Chen et al., 2006). Therefore, finding new methods for producing SnO_2 with orthorhombic structures, such as by pressure tuning (Haines & Leger, 1997), is of particular interest in the sensor industry. In addition, studies suggest that nanostructured SnO_2 might exhibit significantly enhanced performance for certain gas-sensing applications than thick films or bulk materials (Wang et al., 2008). Therefore, many nanostructured SnO_2 of different morphologies, including nanoparticles, nanowires, nanorods and nanobelts, have been synthesized (Calestani et al., 2005; Calestani et al., 2005; Zhou et al., 2006) and their optical and electrochemical properties evaluated. Spectroscopic studies such as Raman measurements (Sun et al., 2003) and photoluminescence (Zhou et al., 2006) show that SnO_2 nanobelts exhibit unique optical properties that are different than those from bulk materials. These recent studies motivated us to undertake the high-pressure investigations on the behaviors of one-dimensional nanostructured SnO_2, resulting in the observation of novel, and unexpected nano-effects.

3.2 Raman spectrum of SnO_2 nanobelts

Raman measurements were performed on SnO_2 nanobelts with selected spectra depicted in Fig. 4. SnO_2 nanobelts at ambient pressure had a regular rutile-type structure (space group $P4_2/mnm$ or D_{4h}^{14}, Z=2) and, therefore, the irreducible representation predicted the Raman active modes to be A_{1g}, B_{1g}, B_{2g} and E_g, with three bands observed at 473 cm^{-1} (E_g), 631 cm^{-1} (A_{1g}) and 773 cm^{-1} (B_{2g}), consistent with previous Raman measurements on nanostructured SnO_2 (Sun et al., 2003). Additional weak Raman bands at 500 cm^{-1} and 692 cm^{-1} can be assigned as A_{2u} (TO) and A_{2u} (LO) modes, both of which are IR active, whereas the band at 544 cm^{-1} was a Raman forbidden B_{1u} mode. These abnormal Raman bands are characteristic of SnO_2 nanobelts and are not observed in the Raman spectrum of bulk SnO_2 (Sun et al., 2003). Four additional Raman active modes were observed below 300 cm^{-1} (not shown here), which can be attributed to the impurities of the substoichiometric Sn_2O_3/Sn_3O_4 phases in the synthetic process (Wang et al., 2007). Interestingly, no strong Raman active modes were observed for the SnO_2 nanowires, which is in contrast to a Raman study by Zhou et al. (Zhou et al., 2006) on single crystalline SnO_2 wires. It is well known that the optical properties of nanomaterials, especially their Raman features, are very sensitive to a number of factors including size, morphology, synthetic route, purity, as well as short-range structures and environment (Gouadec & Colomban, 2007). As a result, different Raman measurements on the same materials (e.g., various metal oxides) but with different nano-parameters have been reported and analyzed extensively (Arora et al., 2007; Gouadec & Colomban, 2007). Upon compression, all SnO_2 nanobelts Raman modes exhibited a blue shift with decreasing intensities along with profile broadening. At the highest pressure, only the A_{1g} mode was observed to have a significantly broadened profile (middle spectrum of Fig. 4). Upon decompression, the Raman profiles changed very gradually as the pressure decreased. As the SnO_2 nanobelts returned to ambient pressure (lower spectrum of Fig. 4), the E_g and B_{2g} modes were recovered but the bands remained broadened. These

observations indicate the partial reversibility of the SnO_2 nanobelts optical responses to compression and decompression, which is coincident with the pressure-induced morphology modifications. The SEM images obtained before compression (Fig. 1a), and after decompression (Fig. 1b), suggest that the belts are crushed to shorter sections that are thicker than the original belts before compression. In contrast, the SnO_2 nanowires exhibited more dramatic changes in morphology as a result of compression, i.e., the wire shapes were no longer recognizable (Fig. 1d).

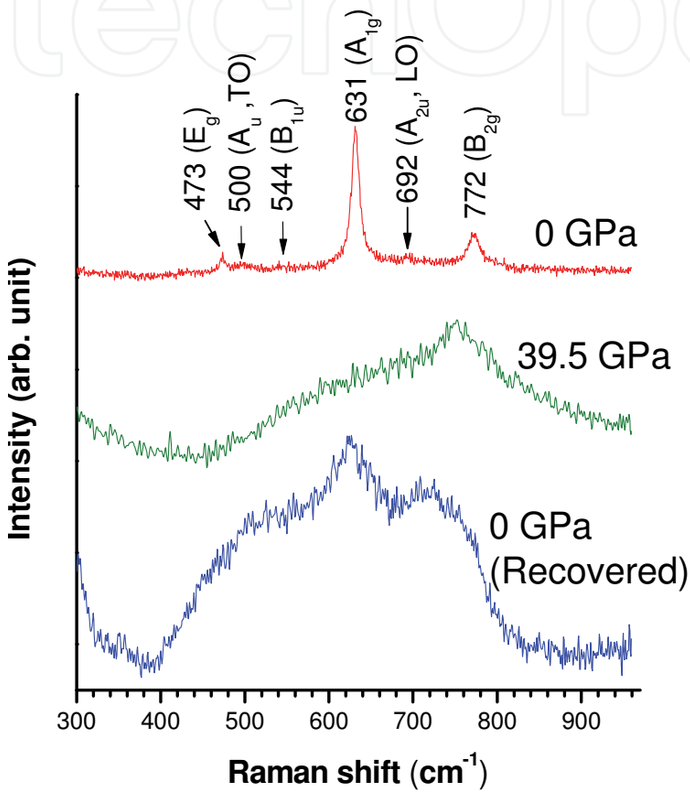

Fig. 4. Raman spectra of SnO_2 nanobelts in the spectral region of 300 to 1000 cm^{-1} collected at ambient pressure (top), at 39.5 GPa (middle) and upon decompression (bottom). The assignments of the observed Raman modes are labeled above the ambient-pressure spectrum. (From Dong and Song, 2009)

3.3 X-ray diffraction of SnO_2 nanobelts

In situ high-pressure angle dispersive X-ray diffraction measurements were performed on SnO_2 nanobelts on compression up to 38 GPa followed by decompression. Representative diffraction patterns are depicted in Fig. 5. Fig. 6 shows the quantitative analysis of the nanobelts diffraction patterns at 14.8, 19.2 and 31.8 GPa and upon complete decompression (i.e., recovered). Starting at ambient pressure, the diffraction pattern of SnO_2 nanobelts indicates an excellent crystalline phase that adopts a rutile structure ($P4_2/mnm$) that is the same as that for the bulk material (Haines & Leger, 1997), with cell parameters of a=4.7218Å and c=3.1802 Å. All the diffraction patterns can be indexed with a single rutile-type phase

until compressed to near 15 GPa (Fig. 6a). The broadening of the (101), (200) and (211) reflections of the rutile phase suggests that an orthorhombic phase has formed ($CaCl_2$-type structure with space group *Pnnm*). Rietveld refinement suggests that there was only a slightly modified cell parameter from the rutile structure: a=4.6543 Å, b=4.5744 Å and c=3.1483 Å. This pressure-induced phase transformation was similar to that observed with bulk SnO_2 (Haines & Leger, 1997), but the transformation pressure was higher. SnO_2 nanobelts existed in this single phase up to 19.2 GPa beyond which new phase transformations were observed (Fig. 6b). The new reflections at 2θ of 6.606° and 8.129° were characteristic of a new orthorhombic α-PbO_2 phase (*Pbcn*) at (110) and a cubic fluorite phase ($Pa\bar{3}$) at (111) directions, respectively. From 19.2 GPa to the highest pressure in the present study, SnO_2 existed as a mixture of these three phases (Fig. 6c). This observation is in strong contrast to the phases observed for bulk SnO_2 materials, in which both the $CaCl_2$-type and α-PbO_2 phases are reported to exist between 12 and 21 GPa (Haines & Leger, 1997). Upon decompression, the three-phase mixture was found to persist down to 7.5 GPa, when the cubic fluorite phase disappeared, with a subsequent back transformation to the rutile structure. Upon complete decompression, the SnO_2 nanobelts were composed of mixtures of rutile and α-PbO_2 phases (Fig. 6d).

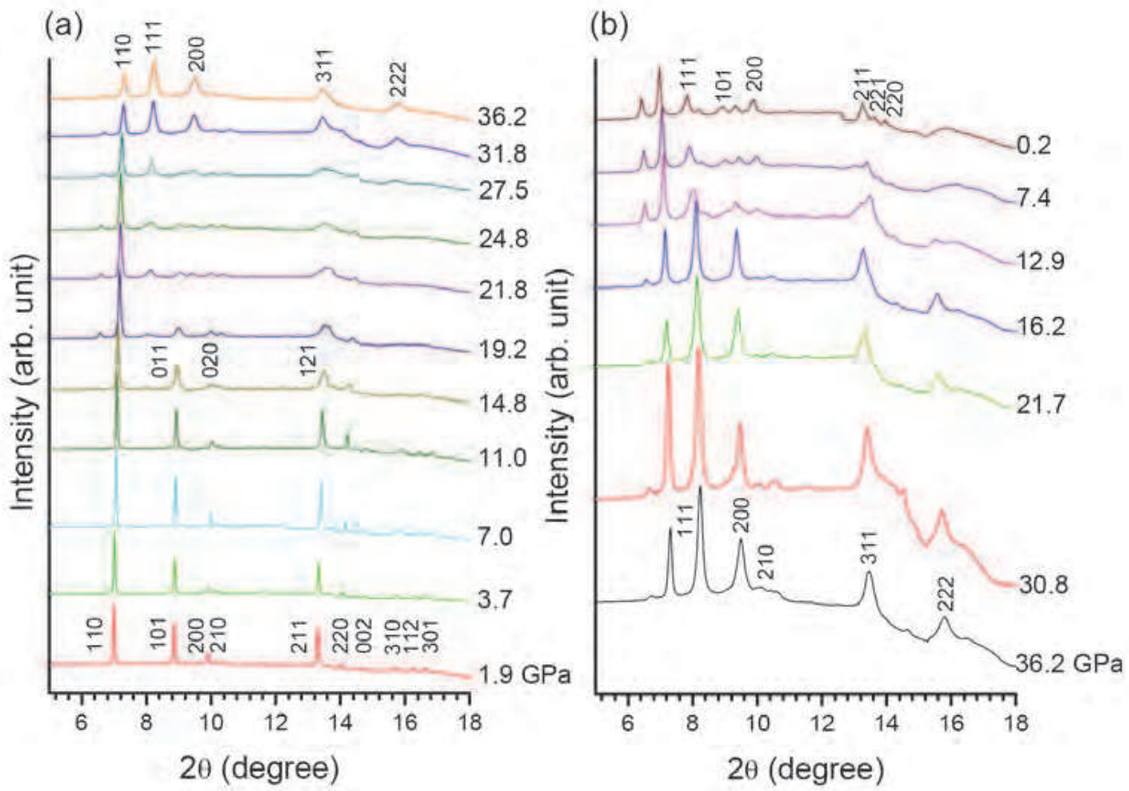

Fig. 5. X-ray diffraction patterns of SnO_2 nanobelts at selected pressures on compression (a) and decompression (b). Pressures in GPa are labeled along each pattern. The Miller indices are shown for the tetragonal structure at 1.9 GPa, the orthorhombic structure at 14.8 GPa and the cubic structure at 36.2 GPa on compression, and at 36.2 GPa and 0.2 GPa on decompression, respectively.

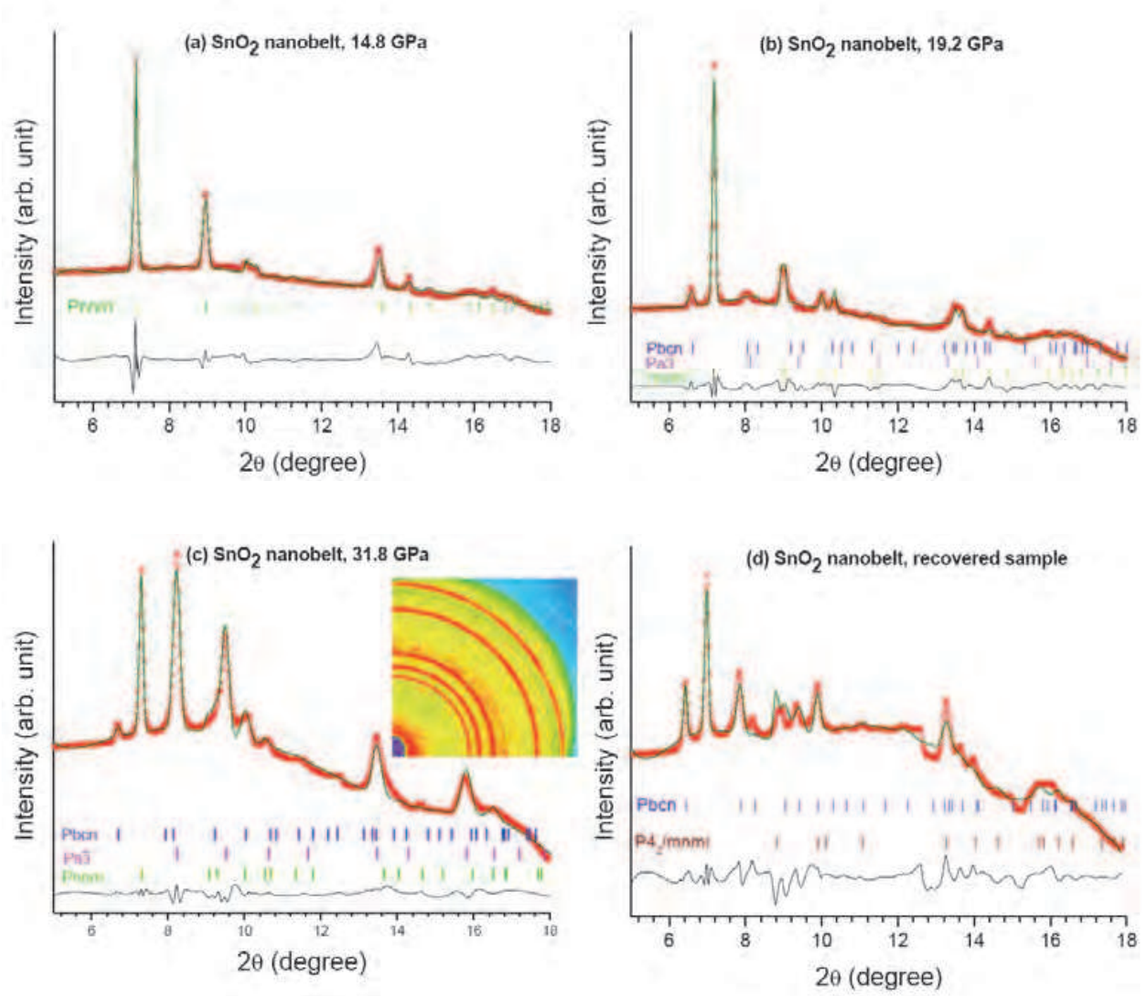

Fig. 6. Rietveld refinement of X-ray diffraction patterns of SnO_2 nanobelts at 14.8 GPa (a), 19.2 GPa (b), 31.8 GPa (c) and from recovered sample (d). The inset in (c) shows the original 2D Debye-Scherrer patterns with one quadrant. The red cross is experimental X-ray intensity whereas the green solid line is the calculated diffraction pattern based on refinement with the black curve at the bottom showing the difference between the calculated and observed intensities. The vertical bars with different colors indicate the characteristic reflections of different phases labeled in the front.

3.4 X-ray diffraction of SnO_2 nanowires

The X-ray diffraction patterns SnO_2 nanowires at selected pressures upon both compression and decompression are depicted in Fig. 7. The Rietveld refinement analysis for patterns at pressures of 14.8, 20.0 and 34.4 GPa and upon complete decompression is shown in Fig. 8. Upon compression and decompression, as can be seen, SnO_2 nanowires exhibit unexpected

pressure responses that are different than those for nanobelts or bulk materials. Starting with the same rutile structure (e.g., Fig. 8a), transformation to a $CaCl_2$-type orthorhombic structure (Fig. 8b) was observed only when it was compressed to 17 GPa, which is a higher transition pressure than that for the nanobelts and much higher (ΔP > 5GPa) than that for the bulk materials. When further compressed to 25 GPa, a fluorite-type phase was found to contribute to the overall diffraction pattern and coexisted with the $CaCl_2$ type phase all the way to the highest pressure. A striking observation that the α-PbO_2 phase was missing in the entire compression region was noted as shown in the Rietveld refinement analysis of the diffraction pattern, which unambiguously suggests that the SnO_2 nanowires are composed of only $CaCl_2$-type and fluorite-type phases at 34.4 GPa (Fig. 8c). Upon decompression, the $CaCl_2$-type phase transformed back to the rutile-type phase at 16 GPa, which is much earlier than that observed for either nanobelts or bulk materials. Further decompression results in more surprising transformations - the fluorite-type phase persists all the way to near-ambient pressure, whereas the α-PbO_2 phase that was missing during compression was observed when it was decompressed to 10.6 GPa and was recovered at ambient pressure (Fig. 8d).

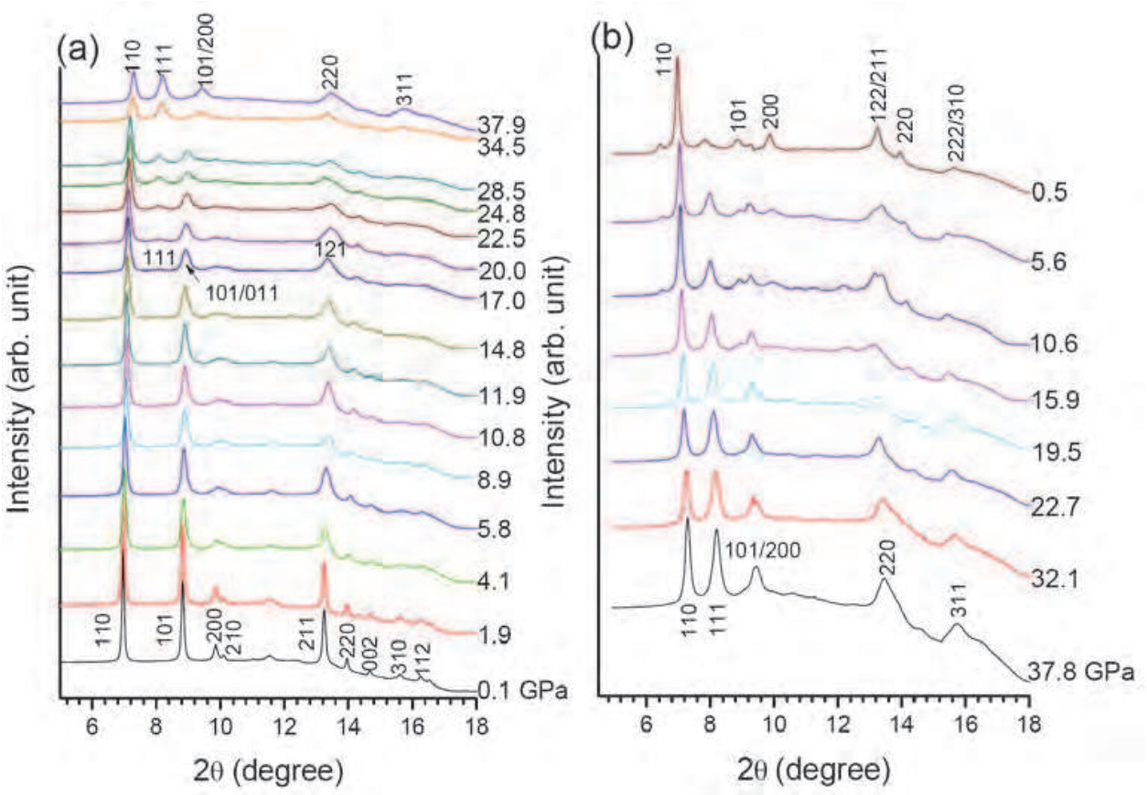

Fig. 7. X-ray diffraction patterns of SnO_2 nanowires at selected pressures on compression (a) and decompression (b). The legends follow Fig. 5.

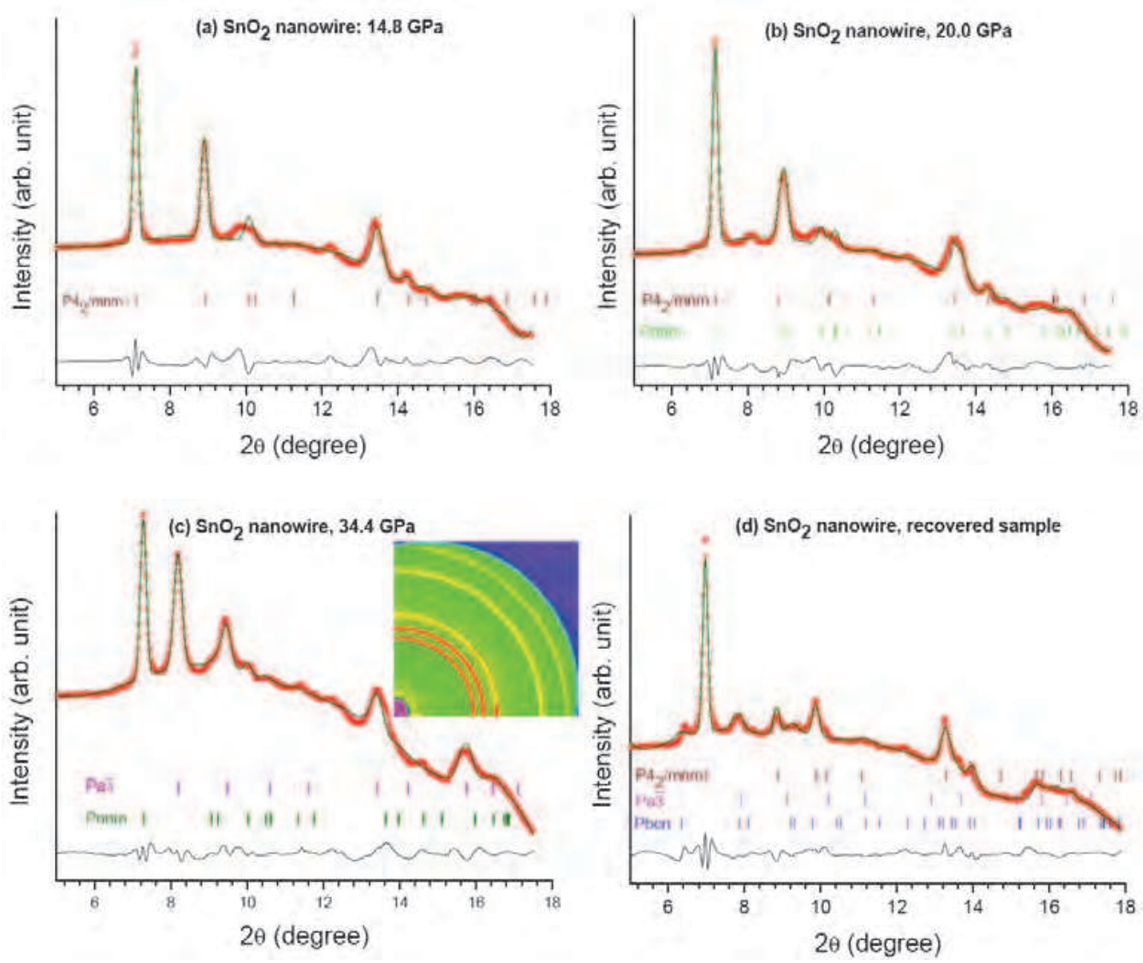

Fig. 8. Rietveld refinement of X-ray diffraction patterns of SnO_2 nanowires at 14.8 GPa (a), 20.0 GPa (b), 34.4 GPa (c) and from recovered sample (d). The legends follow Fig. 6.

3.5 Equation of states

Rietveld refinement performed on all diffraction patterns indicated that the rutile and $CaCl_2$-type phases were the dominant phases both for nanobelts and nanowires, whereas the α-PbO_2 and flurorite phases contribute to the mixed phases only to a certain extent. Therefore, we fit the third-order Birch equation of state (EOS) based on only the dominant phases of nanobelts and nanowires (Fig. 9) to estimate the compressibility using (Birch, 1978):

$$P = \frac{3}{2}B_0\left[\left(V/V_0\right)^{-7/3} - \left(V/V_0\right)^{-5/3}\right] \times \left\{1 + \frac{3}{4}\left(B_0' - 4\right)\left[\left(V/V_0\right)^{-2/3} - 1\right]\right\} \quad (2)$$

where V_0 is the original cell volume at ambient pressure, and V is the cell volume at pressure P. B_0 and B_0' are the bulk modulus and its first pressure derivative, respectively, at ambient pressure.

The bulk modulus and its first derivative were found to be B_0=169.3 GPa and B′=8.4 for the nanobelts whereas those for the nanowires were B_0=225.3 GPa and B′=8.1, respectively. We note that the compressibility of the nanobelts was significantly higher than that for the bulk material (B_0= 204 GPa, B′= 8.0) (Haines & Leger, 1997), whereas the nanowires were less compressible.

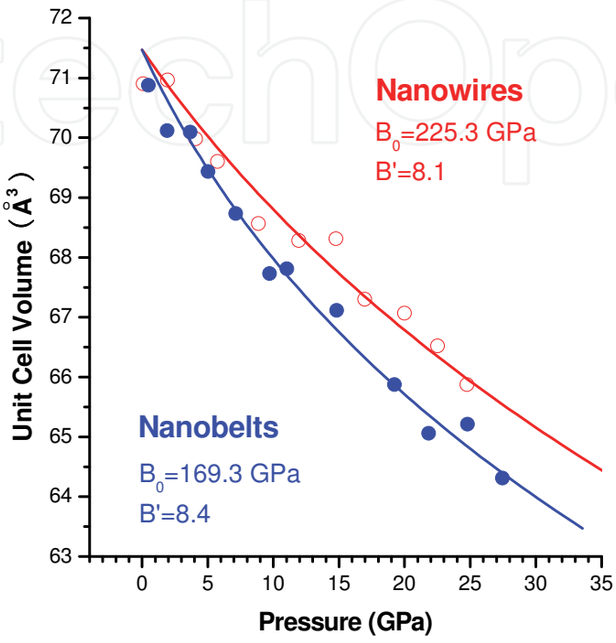

Fig. 9. Pressure-volume relations for SnO_2 nanowires (open circles) and nanobelts (solid circles). The solid lines are fittings using 3rd order Birch equation of state (see text).

The size- and morphology-induced alteration of SnO_2 compressibility characterized by bulk moduli can be understood in parallel with other nanomaterials. CeO_2 nanoparticles exhibit a prominent enhancement of the bulk modulus compared with that for bulk materials (Wang et al., 2001; Wang et al., 2004), whereas no obvious difference in compressibility was observed for ZnS nanocrystals (Jiang et al., 1999). In contrast, the compressibility of PbS and γ-Al_2O_3 (Chen et al., 2002) was found to increase with decreasing nanoparticle size. Furthermore, strongly contrasting compressibility was observed for TiO_2 nanoparticles, i.e, the bulk modulus of the rice-shaped particles was reduced whereas that of the rod-shaped particles was enhanced by more than 50% relative to that of the bulk materials (Park et al., 2008). Therefore, multiple factors determine the mechanical properties of nanomaterials. In this case, by carefully examining SnO_2 nanobelts at ambient pressure using SEM and Raman imaging (Wang et al., 2007), other tin oxides (SnO_x) attached to the nanobelt surface could contribute to the defect in the SnO_2 crystal lattice and may therefore decrease the stiffness. Compared with nanobelts, SnO_2 nanowires carry much fewer or no defects and are more strictly one-dimensional in morphology, which may correlate with their general size-dependent compressibility (Wang et al., 2001). These arguments are corroborated by a previous comparative study of nanobelts and nanowires (Calestani et al., 2005).

3.6 Discussion

Fig. 10 summarizes the strongly contrasting pressure-induced phase transformations of SnO_2 nanobelts and nanowires compared with bulk materials. The differences in the pressure-induced phase transitions between nanostructured and bulk SnO_2 materials have been observed for other morphologies, primarily nanoparticles. However, contrasting results were reported by different groups - He et al. found that transition pressure increases with decreasing SnO_2 nanocrystal size (He et al., 2005), whereas Jiang et al. observed no obvious size-dependent transition pressure differences (Jiang et al., 2001). For other nanostructured materials such as oxides, sulfides or elements, transition pressure shifts have been found to go in both directions. The majority of these nanomaterials (e.g., CdSe (Tolbert & Alivisatos, 1994; Tolbert & Alivisatos, 1995), ZnS (Jiang et al., 1999) and PbS (Jiang & Gerward, 2000)) exhibit higher transition pressures than bulk materials do and their transition pressures also increase with decreasing nanocrystal size (Tolbert & Alivisatos, 1995). However, other nanocrystal oxides, such as γ-Fe_2O_3 (Jiang et al., 1998) and CeO_2 (Rekhi et al., 2001), have reduced transition pressures. The general understanding of the 'size' effect in pressure-induced transformations is used to examine a thermodynamic function, i.e., the Gibbs free energy change (ΔG) with the major contributing factors: the ratio of the volume collapse ($P\Delta V$), the surface energy differences ($A\Delta\gamma$) and the internal energy differences (ΔU) (Jiang, 2004; Wang et al., 2005). It is believed that enhanced transition pressures in nanomaterials indicate that surface energy differences are playing a dominant role, whereas reduced transition pressures might be associated with a compression process overwhelmed by volume collapse. The 'size' effect also seems to extend to one-dimensional nanomaterials such as ZnS nanobelts (Wang et al., 2005). Indeed, it was found that the reduced ZnS nanobelt thickness resulted in a higher transition pressure (Wang et al., 2005). Therefore, these principles can be adopted to explain some of the pressure-induced transformations observed in this study. The higher transition pressures observed both in nanobelts and nanowires indicate that there is a prominent surface energy effect on nanostructured SnO_2. In particular, the onset pressures involving the rutile-to-$CaCl_2$ type transition are approximately 11.8, 15.0 and 17.0 GPa for bulk materials, nanobelts and nanowires, respectively. Because there is no significant change in the unit cell volume in this transition, the contribution of the first factor, i.e., the ratio of the volume collapse to the overall ΔG, is negligible. Considering that the internal energy differences (ΔU) are typically small or negative (Jiang, 2004), the surface energy differences mainly are therefore believed to be responsible for the enhanced transition pressures for nanostructured SnO_2. Gauging from the observed transition pressures, the surface energy differences in the nanowires were estimated to be 62.5% higher than in the nanobelts. Qualitatively, the significantly enhanced nanowire transition pressures can be interpreted by further 'reduced size' from nanobelts with reduced width and thickness. Indeed, the band widths of the nanowire reflections are slightly higher in the nanobelts in general, consistent with the size-induced broadening observed for other nanomaterials (Wang et al., 2004).

In addition to size effects, morphology has also proven to be an important factor for regulating nanomaterial structure and stability, either by early or delayed phase transitions (Wang et al., 2005). However, the drastically contrasting phase stability regions observed for different morphologies of SnO_2, especially for the completely missing α-PbO_2 phase, are

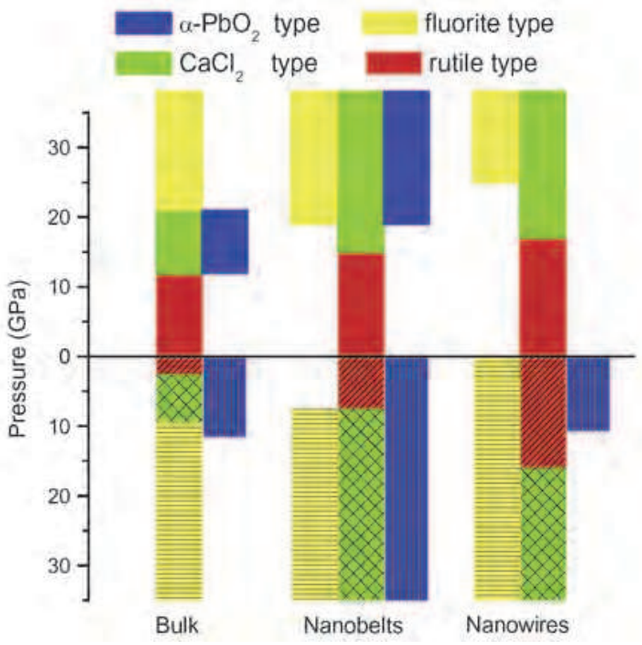

Fig. 10. Summary of pressure-induced phase transformations for SnO_2 nanobelts and nanowires upon compression (plain vertical bars) and decompression (hatched vertical bars) compared with those for bulk SnO_2 material. The different colors label different phases: rutile (red), $CaCl_2$ type (green), flurorite type (yellow) and α-PbO_2 type (blue).

unprecedented. On the basis of the above principles, one may speculate that the α-PbO_2 transition pressure might be significantly elevated (i.e., >> 38 GPa), which requires further experimental and theoretical justification. However, such huge pressure increases may well induce other new SnO_2 phases to form (Shieh et al., 2006). Therefore, the α-PbO_2 phase is likely a metastable phase that cannot simply be interpreted by thermodynamic principles alone. Furthermore, the observed prominent hysteresis, which was characterized by significantly different forward and backward transition pressures, is likely a consequence of different transformation barriers. While the stabilities of difference phases are only determined by thermodynamic functions, the actual transformation pressure may be predominantly governed by kinetics, which scales with the width of the hysteresis. It would therefore be interesting to investigate hysteresis and kinetics as a function of temperature. Indeed, the hysteresis for the nanocrystal CdSe transitions was found to narrow as temperature increased (Chen & Herhold, 1997). The combination of pressure, size, morphology, thermodynamics and kinetics has led to the formation of a multi-dimensional structure-property domain with extremely broad tunabilities. Our findings indicate that certain structures and/or phases can be switched 'on' or 'off' at selected pressure regions with selected morphologies via selected paths. Applying pressure to nanomaterials with different morphologies, therefore, has profound implications for producing controlled structures with desirable properties, such as those for gas sensors whose sensitivity has a preferential correlation to the orthorhombic α-PbO_2-type structure of SnO_2 (Arbiol et al., 2008). However, detailed transformation mechanisms, especially the origins of the surprising reversibility and metastability require further theoretical investigation.

4. GaN nanowires under high pressures

4.1 Properties, structures, and applications of GaN

Gallium nitride (GaN) is a wide band gap semiconductor (3.5 eV) of great technological importance due to its potential applications in high brightness blue/green light emitting diodes (LEDs) and room temperature blue laser (Nakamura et al., 1997). These applications usually require GaN in the wurtzite and zinc blende phases depending on the synthetic techniques (Lei et al., 1992). In addition, GaN is also characterized to have high hardness, low compressibility, high ionicity and high thermal conductivity. These properties make GaN a promising candidate for optoelectronic devices operating under extreme conditions such as at high pressure (Liu et al., 1999). At ambient condition, GaN crystallizes in a wurtzite (B4) structure with a space group of $P6_3mc$ (Schulz & Thiemann, 1977). It is well established that GaN transforms to the rocksalt (B1) structure (space group $Fm\bar{3}m$) at high pressure as suggested by recent theoretical and experimental reports (Cui et al., 2002; Jorgensen et al., 2003; Munoz & Kunc, 1991; Pandey et al., 1994; Perlin et al., 1992; Saib & Bouarissa, 2007; Ueno et al., 1994; Xia et al., 1993; Xiao et al., 2008). For instance, Perlin et al. identified such phase transformation at 47 GPa using Raman scattering and X-ray absorption spectroscopy (Perlin et al., 1992). By synchrotron energy-dispersive X-ray diffraction, Xia et al. reported the first observation of rocksalt phase at an onset pressure of 37 GPa (Xia et al., 1993). Additional later studies confirmed that GaN with different forms all underwent the wurtzite to rocksalt transformation on compression, however, with large discrepancies in transition pressures (e.g., 42-54 GPa for experimental results (Halsall et al., 2004; Perlin et al., 1992; Ueno et al., 1994) and 37-55 GPa for some theoretical studies (Abu-Jafar et al., 2000; Cai & Chen, 2007; Mujica et al., 2003; Munoz & Kunc, 1991; Pandey et al., 1996; Serrano et al., 2000)). GaN can also be synthesized in the nanocrystalline form, either as nanowires or as quantum dots (Jorgensen et al., 2003; Liu et al., 2003; Zhou et al., 2005). Compared to bulk GaN, nanostructured GaN exhibits attractive properties and thus enhanced performance for applications such as optoelectronic devices because of its excellent tunability as a direct band gap semiconductor (Qian et al., 2005). Therefore, studies on structural tuning of nano-GaN such as by the application of pressure in comparison with the bulk materials are of fundamental interests. To date, very few experiments were performed on nanostructured GaN at high pressure. Only Jorgensen et al. has investigated the phase transformations and compressibility of GaN nanocrystals in comparison with the bulk GaN using X-ray diffraction (Jorgensen et al., 2003). Here we discuss the *in situ* high-pressure X-ray diffraction measurements on one-dimensional nanostructured GaN in the form of zigzagged nanowires where interesting, abnormal pressure behaviors were observed.

4.2 GaN nanowires upon compression

Selected X-ray diffraction patterns of GaN nanowires collected upon compression to 65 GPa are shown in Fig. 11a. The X-ray diffraction pattern collected at near ambient pressure (i.e., 0.5 GPa) can be indexed with a hexagonal wurtzite structure ($P6_3mc$) with cell parameters a=b=3.1916 Å and c=5.1733 Å, consistent with the previous X-ray diffraction measurement on GaN nanowires (Zhou et al., 2005). In contrast to the diffraction pattern of nanocrystalline GaN which is characterized with significantly broadened reflection profiles (Jorgensen et al., 2003), however, the narrow and sharp reflections for GaN nanowires here suggest an excellent crystalline phase that resembles bulk GaN. Upon compression, the

wurtzite phase was found to persist to 65 GPa indicated by the consistent indexing of the first six reflections associated with this phase. At 55 GPa, a new reflection appeared at 10.4519°, which can be indexed as (2 0 0) for the rocksalt phase, suggesting the onset of phase transformation. The phase transformation can be further evidenced by the depletion of the strong (1 0 0) reflection at the lowest 2θ angle and the dominant reflection (1 0 1) of wurtzite phase which coincides with reflection (1 1 1) of the rocksalt phase. We note that the phase transition pressure of 55 GPa is higher than that in most previous studies for bulk GaN (Ueno et al., 1994; Xia et al., 1993) but lower compared to that for nanocrystalline GaN which was found to be around 60 GPa (Jorgensen et al., 2003). Size and morphology dependent enhancement of transition pressures have been observed in other nanostructured materials (Dong & Song, 2009). Now it is the general understanding that the surface energy that plays an important role in nanostructures contributes to the enhanced transition pressures. The GaN nanowires in the current study had an initial wire-like morphology and converted to smaller nanoparticles on compression with an average size of 50-200 nm as shown in Fig. 2b, resulting an increase of surface area. Comparing with the particle size of nanocrystalline GaN (i.e., 2-8 nm) studied previously (Jorgensen et al., 2003), it can be inferred that surface energy of GaN increased from bulk to nanowires and to nanoparticles with decreasing sizes, giving the corresponding different transition pressures.

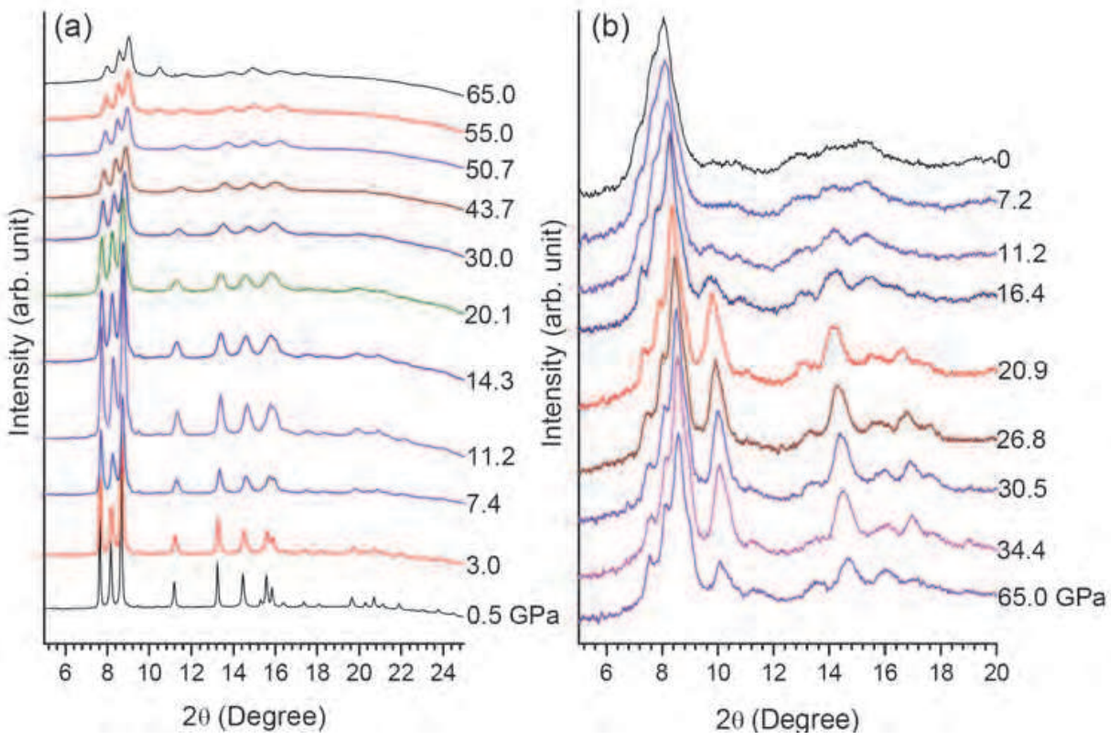

Fig. 11. Angle-dispersive X-ray diffraction patterns (λ=0.3680 Å) of GaN nanowires at selected pressures upon compression (a) and decompression (b). The pressures in GPa are labelled along each pattern.

Another significant difference between this study and previous studies on bulk GaN is that the wurtzite-to-rocksalt transformation for GaN nanowires is far from complete even at 65 GPa. Quantitative Rietveld analysis of GaN nanowires diffraction pattern at 65 GPa shown

in Fig. 12a indicates that wurtzite and rocksalt phases co-exists at this pressure with respective abundance of 88% and 12%. In contrast, an abundance of near 100% for the rocksalt phase was reported for bulk GaN at a pressure less than 60 GPa in most of the previous studies. For example, Perlin et al. found that the wurtzite phase disappears at 54 GPa (Perlin et al., 1992), while Halsall et al. reported such a pressure to be 49 GPa (Halsall et al., 2004). The highest pressure for complete transformation to rocksalt phase for bulk GaN was reported to be 58.8 GPa (Cui et al., 2002) and 60.6 GPa (Ueno et al., 1994), respectively. Our observation is consistent with that for nanocrystalline GaN where the wurtzite to rocksalt phase transition was found incomplete even at 63.5 GPa (Jorgensen et al., 2003). Similar situations were also observed in other one-dimensional nanomaterials, such as in multi-wall boron nitride nanotubes (MW-BNNT) (Dong & Song, 2010). The required pressures for the hexagonal-to-wurtzite structural transformation to be completed are 23 GPa for bulk BN and > 35 GPa for MW-BNNTs, respectively, which can be understood from the topological and mechanical aspects of BNNT nanostructures (Dong & Song, 2010). In addition to the intrinsic properties of nanostructures, non-hydrostaticity may also contribute to the "sluggish" phase transformations. We realize that silicone oil used as the pressure transmitting media in this study, which forms a glass phase even at very low pressures (Ragan et al., 1996), is far from ideal. The non-hydrostaticity in manifested by the significant broadening of all reflections especially at high pressures as shown in the Debye-Scherrer 2D

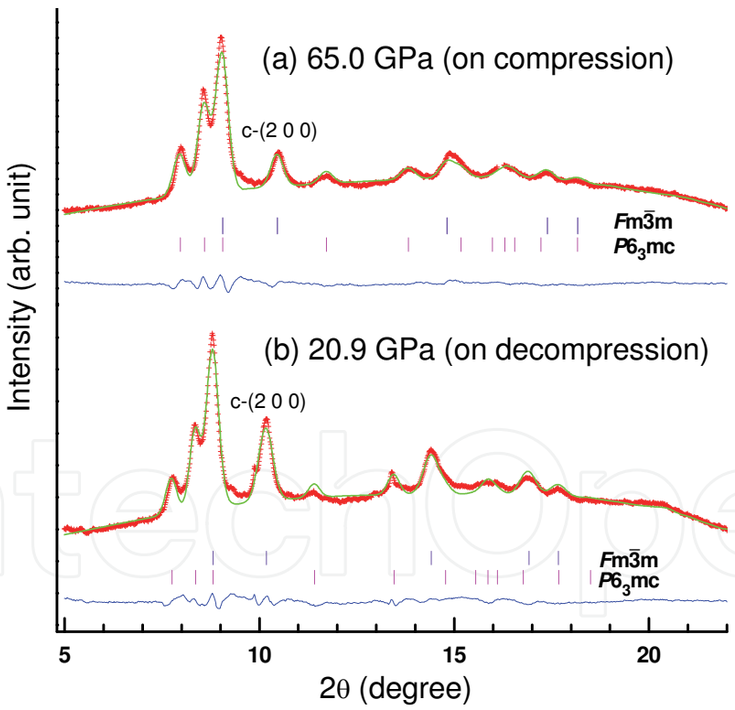

Fig. 12. Rietveld refinement of x-ray diffraction pattern at 65 GPa (a) and 20.9 GPa (b). The redcross is experimental X-ray intensity and the green line is the calculated diffraction patterns based on refinement with the blue curve at the bottom showing the difference between the calculated and observed intensities. The vertical bars denote the indexed reflections for each phase with the space groups labeled beside. The characteristic reflection for the cubic rocksalt phase is labeled as c-(2 0 0). (From Dong and Song, 2010)

diffraction patterns in Fig 13. For instance, the full width at half maximum (FWHM) of reflection (1 0 1) increased dramatically from 0.09° at 0.5 GPa to 0.25° upon compression 65 GPa. Furthermore, severe distortions in the Debye-Scherrer 2D diffraction patterns for reflections (1 0 0), (0 0 2) and (1 0 1) were observed in the high-pressure region (Fig. 13b), indicating pressure-induced enhancement of lattice strain. All these factors may interactively affect the phase stabilities and thus the transformation pressures.

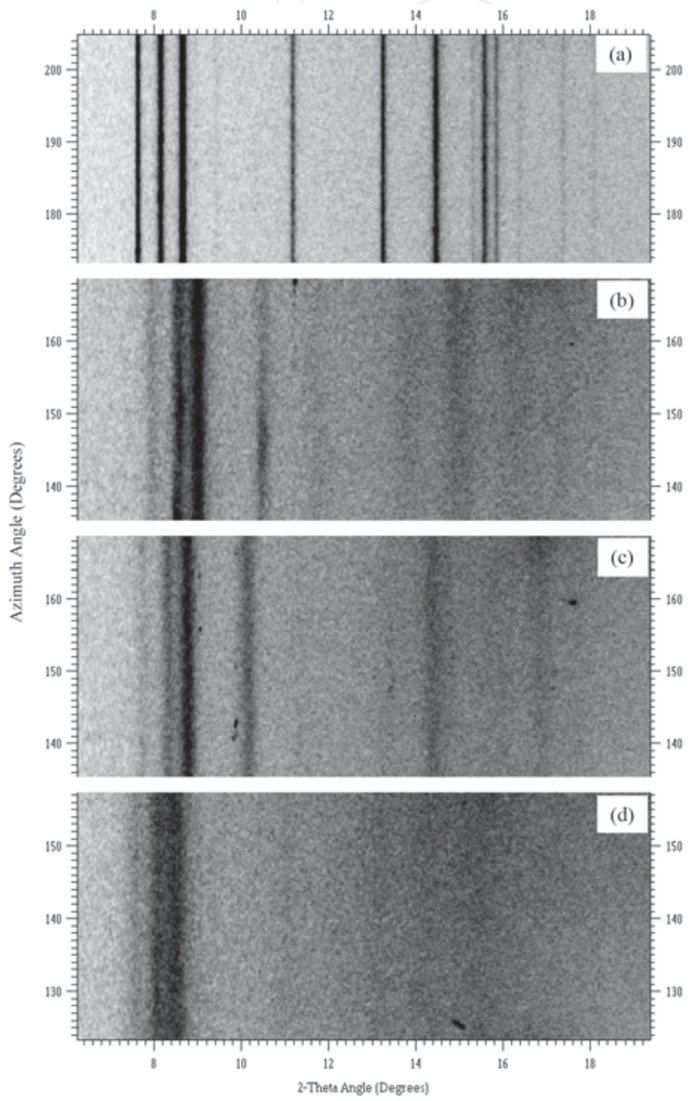

Fig. 13. Debye-Scherrer 2D X-ray diffraction patterns of GaN nanowires at ambient pressure (a), 65 GPa (b), 20.9 GPa upon decompression (c) and ambient pressure upon complete decompression (d).

4.3 GaN nanowires upon decompression

X-ray diffraction patterns of GaN nanowires at selected pressures upon decompression from 65 GPa to the ambient pressure are shown in Fig. 11b. An interesting yet unusual phase transformation was found during decompression. Upon releasing pressure from 65 GPa, the

highest pressure achieved in the current study, the abundance of rocksalt phase was found to increase significantly. For instance, Rietveld refinement (Fig. 12b) suggests that the fraction of rocksalt phase has increased upon releasing the pressure from 12 % at 65.0 GPa to 29% even at 20.9 GPa. Bellow 20.9 GPa, the rocksalt phase gradually transforms back to the wurtzite phase, but was retained even at very low pressures (e.g., <16.4 GPa) as indicated by the noticeable intensity of the (2 0 0) reflection as the dominant reflection of the rocksalt phase. The recovered phase at ambient pressure can be identified as a single wurtzite phase, but the significantly broadened diffraction pattern (Fig. 13d) suggests pressure-induced reduction of the grain size, consistent with the SEM image of the recovered GaN nanomaterial (Fig. 2b). All the previous studies found that B4-B1 phase transformation is reversible for both bulk GaN and nanocrystalline GaN (Cui et al., 2002; Halsall et al., 2004; Perlin et al., 1992) indicating that the wurtzite phase is thermodynamically stable in the low pressure region. However, the strongly contrasting, unprecedented decompression behavior of GaN nanowires exhibiting a large hysteresis suggests that the rocksalt phase is a metastable phase. Prominent hysteresis, which was characterized by significantly different forward and backward transition pressures, is likely due to different kinetic barriers that impede the sharp transitions often involving a metastable phase. Here, we note that this phase of GaN behaves similarly as one of the high-pressure phases (i.e., α-PbO_2 phase) for SnO_2 nanowires (Dong & Song, 2009).

4.4 Equation of state

The unit cell parameters of GaN nanowires at different pressures are plotted in Fig. 14a with the unit cell volume against the pressure for the wurtzite phase plotted in Fig. 14b in comparison with previous studies. As can be seen, the unit cell parameters, the a/c ratio, and the corresponding P-V curve of GaN nanowires exhibit a noticeable discontinuity in the pressure region of 11-20 GPa. In the low pressure region (i.e., < 11 GPa), the equation of state (EOS) for GaN nanowires is almost identical for that of bulk GaN material. Above 11 GPa, obvious change in the P-V relation of GaN nanowires suggest a smaller compressibility or larger bulk modulus. Comparing with previously established EOS for bulk GaN (B_0=187-237 GPa) (Jorgensen et al., 2003; Ueno et al., 1994), and for nanocrystalline GaN (B_0=319 GPa)(Jorgensen et al., 2003), the bulk modulus for GaN nanowires in the pressure region above 20 GPa is estimated to be in between, consistent with that an increase of the surface area may enhance the bulk modulus. This observation can be further understood from the fact the GaN nanowires break into nanoparticles when the external stress surpasses the yield strength at around 20 GPa, resulting in the size-induced enhancement of the bulk modulus. The correlation between the reduction of the particle size and the increasing bulk modulus has been found in other nanomaterials, such as AlN nanocrystals (Wang et al., 2004). A similar discontinuity was also found in the P-V curve for nanocrystalline CeO_2.(Wang et al., 2004) However, a decrease in the bulk modulus of nanocystalline CeO_2 was found above ~20 GPa, a pressure that was believed to signify the onset of a size-induced weakening of the elastic stiffness of nanocrystalline CeO_2. Therefore, the discontinuity in the EOS for both nanocystalline CeO_2 and GaN nanowires can be understood from the nano-size effect while the different shapes of the EOS curves may be associated with opposite pressure-induced changes in particle size. It is probable, too, that the P-V behavior observed in the region of 11-20 GPa is associated with the combined effect of the original nanowires and the yield-generated nanoparticles. The high yield strength observed in the GaN nanowires thus

furthers the understanding of the morphology-tuned improvement in yield strength and hardness in hard materials applications. Moreover, the choice of silicone oil as the pressure-transmitting medium may also contribute to the discontinuity observed in the P-V curve. An anomalous behavior inherent in silicone oil at ~12 GPa, which is believed to be the result of phase transition (Chervin et al., 1995; Klotz et al., 2009), seems to have further complicated the abnormal behavior of GaN nanowires in the pressure region of 11-20 GPa. It would therefore be interesting to use better pressure transmitting media, such as helium, to study compressibility of GaN nanowires in a broader hydrostatic pressure region.

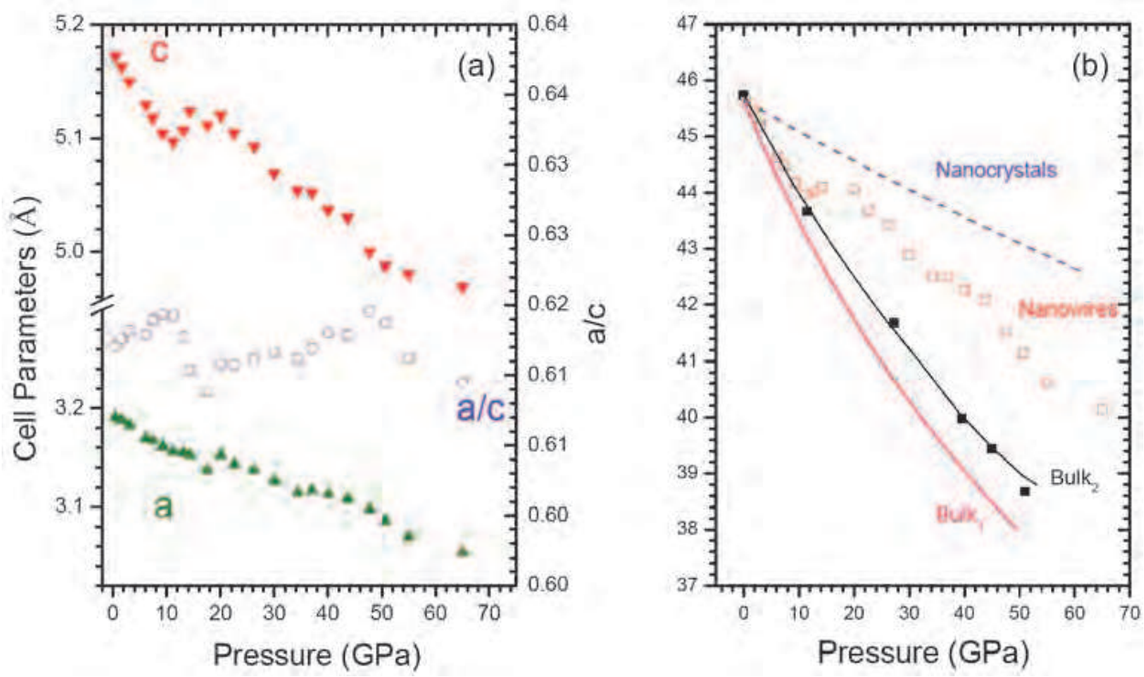

Fig. 14. Unit cell parameters of GaN nanowires as a function of pressure (a) and unit cell volume as a function of pressure for GaN nanowires (open squares) in comparison with that for bulk and nanocrystal GaN (b). Solid lines are fitted EOS curves for bulk GaN using bulk moduli of 187 GPa ($bulk_1$) and 237 GPa ($bulk_2$) from (Jorgensen et al., 2003) and (Ueno et al, 1994) respectively. The dashed line is fitted EOS curve for nanocrystalline GaN using bulk modulus of 319 GPa from (Jorgensen et al., 2003).

5. Summary

In summary, two one-dimensional inorganic materials with various morphologies and sizes were investigated under high pressures. In particular, pressure-induced structural evolutions in nanostructured SnO_2 in the form of nanobelts and nanowires were studied in diamond anvil cells using Raman spectroscopy, angle dispersive X-ray diffraction and SEM. We found that nanostructured SnO_2 exhibits drastically disproportionate high-pressure behaviors compared with bulk materials, which suggests that nanostructured SnO_2 has significantly different optical, chemical and mechanical properties. These morphology-induced differences for some of the phase transformations can be explained by surface energy differences as the dominant thermodynamics factor, while other phases are primarily mediated by kinetics.

These principles may serve as a general guideline for producing novel functional materials with desired stability and/or metastability that may yield promising industrial applications, particularly for semiconductor and chemical sensor uses.
For GaN nanowires, we have investigated high-pressure structures and properties of the first one-dimensional nanostructured GaN using angle-dispersive X-ray diffraction in situ. A wurtzite to rocksalt phase transformation is observed to start at 55 GPa and but is far from complete even at pressures up to 65 GPa. Upon decompression, the abundance of the rocksalt phase was found to increase and then decrease until ambient pressure, at which only the wurtzite phase was recovered, indicating a reversible transformation but with large hysteresis. A discontinuity in the EOS for GaN nanowires is found in the pressure region of 11-20 GPa. These abnormal pressure behaviors of GaN nanowires were compared with previous high pressure studies on bulk and nanocrytalline GaN and can be understood from the nano-size and morphology dependent thermodynamic and kinetic properties of GaN nanowires with the complication of the nonhydrostatic conditions.

6. Future perspectives

Despite that interesting high-pressure behaviors of the two inorganic nanowires were observed and analyzed, more in-depth understanding of these unusual behaviors at quantitative level is still needed. In strong contrast to the extensive high-pressure studies on zero-dimensional nanoparticles, only very few one-dimensional inorganic nanomaterials were investigated at high pressures up-to-date as outlined in Table 1. Therefore, further systematic studies on different inorganic 1D nanostructures with different dimensions under different compression conditions are needed. Additional experimental endeavor with more structural characterization approaches aided with theoretical modeling will help to understand and predict the structures, properties, and transformation mechanisms of these nanomaterials and to shed light on their new promising applications.

7. Acknowledgment

This work is supported by a Discovery Grant, a Research Tools and Instruments Grant from Natural Science and Engineering Research Council of Canada, a Leaders Opportunity Fund from Canadian Foundation for Innovation and an Early Researcher Award from Ontario Ministry of Research and Innovation. The authors acknowledge Prof. T. K. Sham for supplying the material, Drs. D. Shakhvorostov and C. Murli for experimental assistance, Drs. J. Hu and Y. Meng for technical assistance, and Drs. H. Liu and K. K. Zhuravlev for helpful discussions. The original experiments were performed at X17C beamline at the National Synchrotron Light Source at Brookhaven National Laboratory and at HPCAT (Sector 16), Advanced Photon Source, Argonne National Laboratory.

8. References

Abu-Jafar, M.; Al-Sharif, A. I. & Qteish, A. (2000). FP-LAPW and pseudopotential calculations of the structural phase transformations of GaN under high-pressure. *Solid State Communications,* Vol. 116, No. 7, pp. 389-393.

Arbiol, J.; Comini, E.; Faglia, G.; Sberveglieri, G. & Morante, J. R. (2008). Orthorhombic Pbcn SnO2 nanowires for gas sensing applications. *Journal of Crystal Growth,* Vol. 310, No. 1, pp. 253-260.

Arora, A. K.; Rajalakshmi, M.; Ravindran, T. R. & Sivasubramanian, V. (2007). Raman spectroscopy of optical phonon confinement in nanostructured materials. *Journal of Raman Spectroscopy,* Vol. 38, No. 6, pp. 604-617.

Birch, F. (1978). Finite Strain Isotherm and Velocities for Single-Crystal and Polycrystalline Nacl at High-Pressures and 300-Degree-K. *Journal of Geophysical Research,* Vol. 83, No. NB3, pp. 1257-1268.

Cai, J. & Chen, N. X. (2007). Microscopic mechanism of the wurtzite-to-rocksalt phase transition of the group-III nitrides from first principles. *Physical Review B,* Vol. 75, No. 13, pp. 12.

Calestani, D.; Lazzarini, L.; Salviati, G. & Zha, M. (2005). Morphological, structural and optical study of quasi-1D SnO_2 nanowires and nanobelts. *Crystal Research and Technology,* Vol. 40, No. 10-11, pp. 937-941.

Calestani, D.; Zha, M.; Zappettini, A.; Lazzarini, L.; Salviati, G.; Zanotti, L. & Sberveglieri, G. (2005). Structural and optical study of SnO_2 nanobelts and nanowires. *Materials Science and Engineering: C,* Vol. 25, No. 5-8, pp. 625-630.

Chen, B.; Penwell, D.; Benedetti, L. R.; Jeanloz, R. & Kruger, M. B. (2002). Particle-size effect on the compressibility of nanocrystalline alumina. *Physical Review B,* Vol. 66, No. 14, pp. 144101.

Chen, C.-C. & Herhold, A. B. (1997). Size dependence of structural metastability in semiconductor nanocrystals. *Science,* Vol. 276, No. 5311, pp. 398-401.

Chen, Z.; Lai, J. K. L. & Shek, C.-H. (2006). Facile strategy and mechanism for orthorhombic SnO_2 thin films. *Applied Physics Letters,* Vol. 89, No. 23, pp. 231902.

Chervin, J. C.; Canny, B.; Besson, J. M. & Pruzan, P. (1995). A Diamond-Anvil Cell for Ir Microspectroscopy. *Review of Scientific Instruments,* Vol. 66, No. 3, pp. 2595-2598.

Cui, Q.; Pan, Y.; Zhang, W.; Wang, X.; Zhang, J.; Cui, T.; Xie, Y.; Liu, J. & Zou, G. (2002). Pressure-induced phase transition in GaN nanocrystals. *Journal of Physics: Condensed Matter,* Vol. 14, No. 44, pp. 11041-11044.

Cui, Q.; Pan, Y.; Zhang, W.; Wang, X.; Zhang, J.; Cui, T.; Xie, Y.; Liu, J. & Zou, G. (2002). Pressure-induced phase transition in GaN nanocrystals. *Journal of Physics-Condensed Matter,* Vol. 14, No. 44, pp. 11041-11044.

Dong, Z. & Song, Y. (2009). Pressure-induced morphology-dependent phase transformations of nanostructured tin dioxide. *Chemical Physics Letters,* Vol. 480, No. 1-3, pp. 90-95.

Dong, Z. & Song, Y. (2010). Abnormal pressure-induced structural transformations of gallium nitride nanowires. *Applied Physics Letters,* Vol. 96, No. 15, pp. 151903.

Dong, Z. & Song, Y. (2010). Transformations of Cold-Compressed Multiwalled Boron Nitride Nanotubes Probed by Infrared Spectroscopy. *Journal of Physical Chemistry C,* Vol. 114, No. 4, pp. 1782-1788.

Gouadec, G. & Colomban, P. (2007). Raman Spectroscopy of nanomaterials: How spectra relate to disorder, particle size and mechanical properties. *Progress in Crystal Growth and Characterization of Materials,* Vol. 53, No. 1, pp. 1-56.

Gouadec, G. & Colomban, P. (2007). Raman spectroscopy of nanostructures and nanosized materials. *Journal of Raman Spectroscopy,* Vol. 38, No. 6, pp. 598-603.

Guo, Q. X.; Zhao, Y. S.; Mao, W. L.; Wang, Z. W.; Xiong, Y. J. & Xia, Y. N. (2008). Cubic to tetragonal phase transformation in cold-compressed Pd nanocubes. *Nano Letters,* Vol. 8, No. 3, pp. 972-975.

Haines, J. & Leger, J. M. (1997). X-ray diffraction study of the phase transitions and structural evolution of tin dioxide at high pressure:Relationships between structure types and implications for other rutile-type dioxides. *Physical Review B,* Vol. 55, No. 17, pp. 11144 -11154.

Halsall, M. P.; Harmer, P.; Parbrook, P. J. & Henley, S. J. (2004). Raman scattering and absorption study of the high-pressure wurtzite to rocksalt phase transition of GaN. *Physical Review B,* Vol. 69, No. 23, pp. 235207

He, Y.; Liu, J. F.; Chen, W.; Wang, Y.; Wang, H.; Zeng, Y. W.; Zhang, G. Q.; Wang, L. N.; Liu, J.; Hu, T. D.; Hahn, H.; Gleiter, H. & Jiang, J. Z. (2005). High-pressure behavior of SnO_2 nanocrystals. *Physical Review B,* Vol. 72, No. 21, pp. 212102.

Hemley, R. J. & Mao, H. K. (2002). Overview of static high pressure science. Proceedings of the International School of Physics, "Enrico Fermi" Course CXLVII (High Pressure Phenomena), IOS Press, Amsterdam.

Hou, D.; Ma, Y.; Gao, C.; Chaudhuri, J.; Lee, R. G. & Yang, H. (2009). Compression of a crystalline ZnO nanotube: An experimental exploration of the B4 to B1 transition mechanism. *Journal of Applied Physics,* Vol. 105, No. 10, pp. 104317-4.

Jacobs, K.; Zaziski, D.; Scher, E. C.; Herhold, A. B. & Alivisatos, P. A. (2001). Activation Volumes for Solid-Solid Transformations in Nanocrystals. *Science,* Vol. 293, No. 5536, pp. 1803-1806.

Jiang, J. Z. (2004). Phase transformations in nanocrystals. *Journal of Materials Science,* Vol. 39, No. 16-17, pp. 5103-5110.

Jiang, J. Z. & Gerward, L. (2000). Phase transformation and conductivity in nanocrystal PbS under pressure. *Journal of Applied Physics,* Vol. 87, No. 5, pp. 2658-2660.

Jiang, J. Z.; Gerward, L.; Frost, D.; Secco, R.; Peyronneau, J. & Olsen, J. S. (1999). Grain-size effect on pressure-induced semiconductor-to-metal transition in ZnS. *Journal of Applied Physics,* Vol. 86, No. 11, pp. 6608-6610.

Jiang, J. Z.; Gerward, L. & Olsen, J. S. (2001). Pressure induced phase transformation in nanocrystal SnO_2. *Scripta Materialia,* Vol. 44, No. 8-9, pp. 1983-1986.

Jiang, J. Z.; Olsen, J. S.; Gerward, L. & Morup, S. (1998). Enhanced bulk modulus and reduced transition pressure in g-Fe_2O_3 nanocrystals. *Europhysics Letters,* Vol. 44, No. 5, pp. 620-626.

Jorgensen, J. E.; Jakobsen, J. M.; Jiang, J. Z.; Gerward, L. & Olsen, J. S. (2003). High-pressure X-ray diffraction study of bulk- and nanocrystalline GaN. *Journal of Applied Crystallography,* Vol. 36, No. 3, pp. 920-925.

Klotz, S.; Chervin, J. C.; Munsch, P. & Le Marchand, G. (2009). Hydrostatic limits of 11 pressure transmitting media. *Journal of Physics D: Applied Physics,* Vol. 42, No. 7, pp. 075413.

Lei, T.; Moustakas, T. D.; Graham, R. J.; He, Y. & Berkowitz, S. J. (1992). Epitaxial-Growth and Characterization of Zincblende Gallium Nitride on (001) Silicon. *Journal of Applied Physics,* Vol. 71, No. 10, pp. 4933-4943.

Li, Q. J.; Liu, B. B.; Wang, L.; Li, D. M.; Liu, R.; Zou, B.; Cui, T.; Zou, G. T.; Meng, Y.; Mao, H. K.; Liu, Z. X.; Liu, J. & Li, J. X. (2010). Pressure-Induced Amorphization and Polyamorphism in One-Dimensional Single-Crystal TiO2 Nanomaterials. *Journal of Physical Chemistry Letters,* Vol. 1, No. 1, pp. 309-314.

Li, Z.; Liu, B.; Yu, S.; Wang, J.; Li, Q.; Zou, B.; Cui, T.; Liu, Z.; Chen, Z. & Liu, J. (2011). The Study of Structural Transition of ZnS Nanorods under High Pressure. *The Journal of Physical Chemistry C,* Vol. 115, No. 2, pp. 357-361.

Li, Z. P.; Liu, B. B.; Li, X. L.; Yu, S. D.; Wang, L.; Hou, Y. Y.; Zou, Y. G.; Yao, M. G.; Li, Q. J.; Zou, B.; Cui, T. & Zou, G. T. (2007). Solvothermal synthesis of ZnS nanorods and their pressure modulated photoluminescence spectra. *Journal of Physics-Condensed Matter,* Vol. 19, No. 42, pp. 8.

Liu, J.; Meng, X. M.; Jiang, Y.; Lee, C. S.; Bello, I. & Lee, S. T. (2003). Gallium nitride nanowires doped with silicon. *Applied Physics Letters,* Vol. 83, No. 20, pp. 4241-4243.

Liu, Z. X.; Goni, A. R.; Syassen, K.; Siegle, H.; Thomsen, C.; Schottker, B.; As, D. J. & Schikora, D. (1999). Pressure and temperature effects on optical transitions in cubic GaN. *Journal of Applied Physics,* Vol. 86, No. 2, pp. 929-934.

Mujica, A.; Rubio, A.; Munoz, A. & Needs, R. J. (2003). High-pressure phases of group-IV, III-V, and II-VI compounds. *Reviews of Modern Physics,* Vol. 75, No. 3, pp. 863-912.

Munoz, A. & Kunc, K. (1991). High-Pressure Phase of Gallium Nitride. *Physical Review B,* Vol. 44, No. 18, pp. 10372-10373.

Muthu, D. V. S.; Midgley, A. E.; Petruska, E. A.; Sood, A. K.; Bando, Y.; Golberg, D. & Kruger, M. B. (2008). High-pressure effects on boron nitride multi-walled nanotubes: An X-ray diffraction study. *Chemical Physics Letters,* Vol. 466, No. 4-6, pp. 205-208.

Nakamura, S.; Senoh, M.; Nagahama, S.; Iwasa, N.; Yamada, T.; Matsushita, T.; Sugimoto, Y. & Kiyoku, H. (1997). Room-temperature continuous-wave operation of InGaN multi-quantum-well structure laser diodes with a lifetime of 27 hours. *Applied Physics Letters,* Vol. 70, No. 11, pp. 1417-1419.

Pandey, R.; Causa, M.; Harrison, N. M. & Seel, M. (1996). The high-pressure phase transitions of silicon and gallium nitride: A comparative study of Hartree-Fock and density functional calculations. *Journal of Physics-Condensed Matter,* Vol. 8, No. 22, pp. 3993-4000.

Pandey, R.; Jaffe, J. E. & Harrison, N. M. (1994). Ab-Initio Study of High-Pressure Phase-Transition in Gan. *Journal of Physics and Chemistry of Solids,* Vol. 55, No. 11, pp. 1357-1361.

Park, S.-W.; Jang, J.-t.; Cheon, J.; Lee, H.-H.; Lee, D. R. & Lee, Y. (2008). Shape-dependent compressibility of TiO_2 anatase nanoparticles. *Journal of Physical Chemistry C,* Vol. 112, No. 26, pp. 9627-9631.

Perlin, P.; Jauberthiecarillon, C.; Itie, J. P.; Miguel, A. S.; Grzegory, I. & Polian, A. (1992). Raman-Scattering and X-Ray-Absorption Spectroscopy in Gallium Nitride under High-Pressure. *Physical Review B,* Vol. 45, No. 1, pp. 83-89.

Qian, F.; Gradecak, S.; Li, Y.; Wen, C. Y. & Lieber, C. M. (2005). Core/multishell nanowire heterostructures as multicolor, high-efficiency light-emitting diodes. *Nano Letters,* Vol. 5, No. 11, pp. 2287-2291.

Ragan, D. D.; Clarke, D. R. & Schiferl, D. (1996). Silicone fluid as a high-pressure medium in diamond anvil cells. *Review of Scientific Instruments,* Vol. 67, No. 2, pp. 494-496.

Rekhi, S.; Saxena, S. K. & Lazor, P. (2001). High-pressure Raman study on nanocrystalline CeO_2. *Journal of Applied Physics,* Vol. 89, No. 5, pp. 2968.

Saha, S.; Gadagkar, V.; Maiti, P. K.; Muthu, D. V. S.; Golberg, D.; Tang, C.; Zhi, C.; Bando, Y. & Sood, A. K. (2007). Irreversible pressure-induced transformation of boron nitride nanotubes. *Journal of Nanoscience and Nanotechnology,* Vol. 7, No. 6, pp. 1810-1814.

Saha, S.; Muthu, D. V. S.; Golberg, D.; Tang, C.; Zhi, C.; Bando, Y. & Sood, A. K. (2006). Comparative high pressure Raman study of boron nitride nanotubes and hexagonal boron nitride. *Chemical Physics Letters,* Vol. 421, No. 1-3, pp. 86-90.

Saib, S. & Bouarissa, N. (2007). Structural phase transformations of GaN and InN under high pressure. *Physica B: Condensed Matter,* Vol. 387, No. 1-2, pp. 377-382.

San-Miguel, A. (2006). Nanomaterials under high-pressure. *Chemical Society Reviews,* Vol. 35, No. 10, pp. 876-889.

Sangaletti, L.; Depero, L. E.; Dieguez, A.; Marca, G.; Morante, J. R.; Romano-Rodriguez, A. & Sberveglieri, G. (1997). Microstructure and morphology of tin dioxide multilayer thin film gas sensors. *Sensors and Actuators B: Chemical,* Vol. 44, No. 1-3, pp. 268-274.

Schulz, H. & Thiemann, K. H. (1977). Crystal structure refinement of AlN and GaN. *Solid State Communications,* Vol. 23, No. 11, pp. 815-819.

Serrano, J.; Rubio, A.; Hernandez, E.; Munoz, A. & Mujica, A. (2000). Theoretical study of the relative stability of structural phases in group-III nitrides at high pressures. *Physical Review B,* Vol. 62, No. 24, pp. 16612-16623.

Shieh, S. R.; Kubo, A.; Duffy, T. S.; Prakapenka, V. B. & Shen, G. (2006). High-pressure phases in SnO_2 to 117 GPa. *Physical Review B,* Vol. 73, No. 1, pp. 014105.

Sun, S. H.; Meng, G. W.; Zhang, G. X.; Gao, T.; Geng, B. Y.; Zhang, L. D. & Zuo, J. (2003). Raman scattering study of rutile SnO_2 nanobelts synthesized by thermal evaporation of Sn powders. *Chemical Physics Letters,* Vol. 376, No. 1-2, pp. 103-107.

Swamy, V.; Kuznetsov, A.; Dubrovinsky, L. S.; McMillan, P. F.; Prakapenka, V. B.; Shen, G. & Muddle, B. C. (2006). Size-dependent pressure-induced amorphization in nanoscale TiO_2. *Physical Review Letters,* Vol. 96, No. 13, pp. 135702.

Tolbert, S. H. & Alivisatos, A. P. (1994). Size dependence of a first order solid-solid phase transition: the wurtzite to rock salt transformation in CdSe nanocrystals. *Science,* Vol. 265, No. 5170, pp. 373-376.

Tolbert, S. H. & Alivisatos, A. P. (1995). High-pressure structural transformations in semiconductor nanocrystals. *Annual Review of Physical Chemistry,* Vol. 46, pp. 595-625.

Ueno, M.; Yoshida, M.; Onodera, A.; Shimomura, O. & Takemura, K. (1994). Stability of the Wurtzite-Type Structure under High-Pressure - Gan and Inn. *Physical Review B,* Vol. 49, No. 1, pp. 14-21.

Wang, B.; Zhu, L. F.; Yang, Y. H.; Xu, N. S. & Yang, G. W. (2008). Fabrication of a SnO_2 nanowire gas sensor and sensor performance for hydrogen. *Journal of Physical Chemistry C,* Vol. 112, No. 17, pp. 6643-6647.

Wang, F.; Zhou, X.; Zhou, J.; Sham, T.-K. & Ding, Z. (2007). Observation of single tin dioxide nanoribbons by confocal Raman microspectroscopy. *Journal of Physical Chemistry C,* Vol. 111, No. 51, pp. 18839-18843.

Wang, Z.; Daemen, L. L.; Zhao, Y.; Zha, C. S.; Downs, R. T.; Wang, X.; Wang, Z. L. & Hemley, R. J. (2005). Morphology-tuned wurtzite-type ZnS nanobelts. *Nature Materials,* Vol. 4, No. 12, pp. 922-927.

Wang, Z.; Saxena, S. K.; Pischedda, V.; Liermann, H. P. & Zha, C. S. (2001). In situ x-ray diffraction study of the pressure-induced phase transformation in nanocrystalline CeO_2. *Physical Review B,* Vol. 64, No. 1, pp. 012102.

Wang, Z. W.; Tait, K.; Zhao, Y. S.; Schiferl, D.; Zha, C. S.; Uchida, H. & Downs, R. T. (2004). Size-induced reduction of transition pressure and enhancement of bulk modulus of A1N nanocrystals. *Journal of Physical Chemistry B,* Vol. 108, No. 31, pp. 11506-11508.

Wang, Z. W.; Zhao, Y. S.; Schiferl, D.; Zha, C. S. & Downs, R. T. (2004). Pressure induced increase of particle size and resulting weakening of elastic stiffness of CeO2 nanocrystals. *Applied Physics Letters,* Vol. 85, No. 1, pp. 124-126.

Watson, J.; Ihokura, K. & Coles, G. S. V. (1993). The tin dioxide gas sensor. *Measurement Science & Technology,* Vol. 4, No. 7, pp. 711-719.

Xia, H.; Xia, Q. & Ruoff, A. L. (1993). High-Pressure Structure of Gallium Nitride - Wurtzite-to-Rock-Salt Phase-Transition. *Physical Review B,* Vol. 47, No. 19, pp. 12925-12928.

Xiao, H. Y.; Gao, F.; Wang, L. M.; Zu, X. T.; Zhang, Y. & Weber, W. J. (2008). Structural phase transitions in high-pressure wurtzite to rocksalt phase in GaN and SiC. *Applied Physics Letters,* Vol. 92, No. 24, pp. 241909.

Yan, X. Q.; Gu, Y. S.; Zhang, X. M.; Huang, Y. H.; Qi, J. J.; Zhang, Y.; Fujita, T. & Chen, M. W. (2009). Doping Effect on High-Pressure Structural Stability of ZnO Nanowires. *Journal of Physical Chemistry C,* Vol. 113, No. 4, pp. 1164-1167.

Zhou, J. X.; Zhang, M. S.; Hong, J. M. & Yin, Z. (2006). Raman spectroscopic and photoluminescence study of single-crystalline SnO2 nanowires. *Solid State Communications,* Vol. 138, No. 5, pp. 242-246.

Zhou, X. T.; Heigl, F.; Murphy, M. W.; Sham, T. K.; Regier, T.; Coulthard, I. & Blyth, R. I. R. (2006). Time-resolved x-ray excited optical luminescence from SnO_2 nanoribbons: Direct evidence for the origin of the blue luminescence and the role of surface states. *Applied Physics Letters,* Vol. 89, No. 21, pp. 213109.

Zhou, X. T.; Sham, T. K.; Shan, Y. Y.; Duan, X. F.; Lee, S. T. & Rosenberg, R. A. (2005). One-dimensional zigzag gallium nitride nanostructures. *Journal of Applied Physics,* Vol. 97, No. 10, pp. 104315.

Nanowires - Fundamental Research

Edited by Dr. Abbass Hashim

ISBN 978-953-307-327-9
Hard cover, 552 pages
Publisher InTech
Published online 19, July, 2011
Published in print edition July, 2011

Understanding and building up the foundation of nanowire concept is a high requirement and a bridge to new technologies. Any attempt in such direction is considered as one step forward in the challenge of advanced nanotechnology. In the last few years, InTech scientific publisher has been taking the initiative of helping worldwide scientists to share and improve the methods and the nanowire technology. This book is one of InTechâ€™s attempts to contribute to the promotion of this technology.

How to reference

In order to correctly reference this scholarly work, feel free to copy and paste the following:

Zhaohui Dong and Yang Song (2011). Novel Pressure-Induced Structural Transformations of Inorganic Nanowires, Nanowires - Fundamental Research, Dr. Abbass Hashim (Ed.), ISBN: 978-953-307-327-9, InTech, Available from: http://www.intechopen.com/books/nanowires-fundamental-research/novel-pressure-induced-structural-transformations-of-inorganic-nanowires

INTECH
open science | open minds

InTech Europe
University Campus STeP Ri
Slavka Krautzeka 83/A
51000 Rijeka, Croatia
Phone: +385 (51) 770 447
Fax: +385 (51) 686 166
www.intechopen.com

InTech China
Unit 405, Office Block, Hotel Equatorial Shanghai
No.65, Yan An Road (West), Shanghai, 200040, China
中国上海市延安西路65号上海国际贵都大饭店办公楼405单元
Phone: +86-21-62489820
Fax: +86-21-62489821

IntechOpen